Impedance Modeling and Analysis for Piezoelectric Energy Harvesting Systems

Junrui Liang, *Member, IEEE*, and Wei-Hsin Liao, *Senior Member, IEEE*

***Abstract*—In a piezoelectric energy harvesting (PEH) system, the dynamics and harvested power vary with different interface circuits connected. The impedance matching theory was regarded as the theoretical base for the harvested power optimization in the harmonically excited PEH systems. The previous literature started the impedance analyses based on the proposition that the harvested power is maximized when the output impedance of the piezoelectric transducer is matched by the input impedance of the harvesting circuit. Yet, retrospecting to the origin of the impedance matching theory, a philosophical problem is found with this proposition. Moreover, the definition, constraint, and composition of the equivalent impedance in the real (nonlinear) harvesting circuits were not clear as well. This paper clarifies these concepts and provides the impedance modeling and analysis for the PEH systems with different interface circuits, including standard energy harvesting, parallel synchronized switch harvesting on inductor, and series synchronized switch harvesting on inductor. The equivalent impedance network and corresponding mechanical schematics of a general PEH system are proposed. The difference between the PEH equivalent impedance network and the conventional impedance network is discussed. The harvested power is investigated based on this impedance analysis. The analytical results show good agreement with the experiments carried out on a base excited PEH device.**

***Index Terms*—Energy harvesting, equivalent impedance network, harvested power optimization, impedance matching, piezoelectric.**

I. Introduction

VARIOUS sensor techniques can be implemented to measure the physical or environmental parameters in civil infrastructures [1], machines [2], human motions [3], etc. A wireless sensor network consists of different kinds of spatially distributed sensors to monitor a system. In each sensor node, the power dependence on batteries can be eased, if the ambient energy in different forms (e.g., solar, thermal, wind, and vibration) is captured, stored (usually in electrical form), and utilized. Piezoelectric materials, as one sort of the commonly used electromechanical transducers, can be utilized to harvest energy from mechanical vibration sources [4]. In terms of the complexity of the mechanical part, the piezoelectric energy harvesting (PEH) system is the simplest compared to the electromagnetic and electrostatic ones; therefore, it is more welcome in small-scale systems [5].

In PEH systems, the harvested power improvement by modifying the interface circuit is significant. For example, by implementing the parallel synchronized switch harvesting on inductor (P-SSHI) [6] or the series synchronized switch harvest on inductor (S-SSHI) [7], the harvested power can be increased by about 300–400%, compared to the standard energy harvesting (SEH) case. Yet, concerning the power optimization issue, two questions are still open.

1) Given an excitation applied to a specific piezoelectric structure, what is the maximum harvestable power?
2) Is there any existing interface circuit can make this maximum power?

The limit of the harvested power was discussed in some literature by analyzing the ideal work cycle of the electrical part. Liu *et al.* [8] proposed the so-called active PEH, with which they claimed that the harvested power can be increased arbitrarily high without the constraint on power electronics efficiency. Liu *et al.* [9] reached a similar point, but they called their method as velocity-controlled PEH. Earlier than those, Liu *et al.* [10] provided a similar analysis on the ideal work cycle, but they regarded the maximum parameters of a piezoelectric element, e.g., maximum mechanical strain, maximum electrical field, maximum surface charge density, and maximum stress, as the constraints of the electromechanical conversion. There are two common problems in these analyses: 1) These analyses have not considered the reaction of the harvesting circuit to the dynamics of the mechanical part. In real situation, as the extracted power increases, the induced damping effect increases too [11], the vibration magnitude, therefore, is suppressed. Eventually, some of the increase on extracted power will be canceled out. 2) It is not true that the larger the area enclosed by the work cycle, the higher the harvested power. The enclosed area corresponds to the extracted energy in one cycle, which should be subdivided into harvested and dissipated portions [12]. Without considering the *overall dynamics* and the *energy flow* in the system, the discussions on the limit of the harvested power could be misleading.

On the other hand, the impedance approach can be used to analyze the overall dynamics of the PEH systems. It is compatible with the well-established criteria on the power analysis of ac circuits. In the previous literature, it was claimed that the harvested power can be maximized, when the input impedance of the harvesting circuit matches the output impedance of the piezoelectric transducer [13]–[15]. Nevertheless, this

Manuscript received November 24, 2010; revised March 18, 2011; accepted May 31, 2011. Date of publication July 22, 2011; date of current version August 24, 2012. Recommended by Technical Editor J. Wang. This work was supported by a grant from the Research Grants Council of the Hong Kong Special Administrative Region, China, under Project CUHK 414809.

The authors are with the Department of Mechanical and Automation Engineering, The Chinese University of Hong Kong, Hong Kong, China (e-mail: jrliang@mae.cuhk.edu.hk; whliao@cuhk.edu.hk).

Color versions of one or more of the figures in this paper are available online at http://ieeexplore.ieee.org.

Digital Object Identifier 10.1109/TMECH.2011.2160275

1083-4435/$26.00 © 2011 IEEE

proposition has ignored the context of the impedance matching theory, which originally was derived from the series impedance network driven by a voltage source or the parallel impedance network driven by a current source. In addition, three basic factors about the equivalent impedance of a real PEH interface circuit (also the input impedance of its ac–dc stage) were ambiguous in these studies:

1) the definition;
2) its attainable range;
3) its detailed composition.

Without these specifications, the equivalent impedance network of a PEH system would be hardly derived. In addition, there were also conflicts in utilizing the impedance matching theory for power optimization in the electromagnetic energy harvesting systems [16]. On the other hand, the maximum obtainable power is a common concern for different energy harvesting systems [17], [18]. Considering the aforementioned three issues in PEH systems, this paper proposes the impedance modeling and analysis for clarification.

II. Impedance Modeling

Both the modeling techniques for pure mechanical structures and pure electrical circuits are of many options. Take the most investigated cantilevered PEH system with the SEH interface circuit, for example. Its mechanical part is a cantilever beam, which has multiple vibration modes. The structural dynamics can be analyzed with either closed form or numerical solution to the partial differential equations. Its electrical part is a conventional rectifier circuit, which is nonlinear in nature. The circuit waveforms can be obtained with piecewise circuit equations or a circuit simulation software. Yet, when the two domains are bridged by the piezoelectric transducer, the situation becomes complicated. The dynamics of the whole electromechanical device would be hardly modeled accurately with the existing methods. The distributed parameters on mechanical part and nonlinearity on electrical part obstruct the integration of their models. Up to now, most of the studies emphasizing on the mechanical part adopted simplified electrical models [19], [20], while the studies emphasizing on the electrical part adopted simplified mechanical models [6], [21], [22]. The majority of research focused on either mechanical or electrical parts, but not both.

On the other hand, energy flow [12] and impedance matching have been considered from the system level. To utilize the impedance matching, the first problem is: what are the impedances of different parts or components in the system? The equivalent circuit of the linear mechanical part is well established. With the mechanical to electrical analogy, each vibration mode can be equivalently represented by an *RLC* branch in the electrical domain. The corresponding resistance, inductance, and capacitance values can be obtained by experimental identification [23]–[25], analytical method [26], or numerical analysis [27]. Nevertheless, for the electrical part, in most literature, the nonlinear interface circuit was taken as an equivalent resistance, i.e., impedance without an imaginary part [13], [15]. On the other hand, Brufau-Penella and Puig-Vidal [14] regarded it as a complex impedance. They proposed the complex conjugate impedance matching, rather than resistive impedance matching. However, they did the matching with a resistor and an inductor, whose values are able to be arbitrarily chosen, instead of considering the equivalent impedance of a real harvesting interface circuit. How to determine the equivalent impedance of the electrical part in a PEH system is one of the keys for the modeling and analysis in this study.

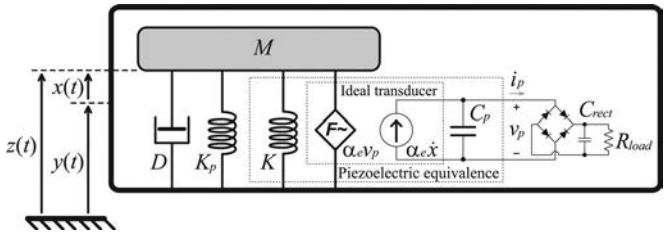

Fig. 1. SDOF schematic representation of a base excited PEH device.

A. Impedance of the Mechanical Part

Fig. 1 gives the single-degree-of-freedom (SDOF) schematic representation of a base excited PEH device, where M, D, K, and K_p represent the equivalent mass, mechanical damping (dissipation), substrate stiffness, and piezoelectric short circuit stiffness, respectively; C_p is the piezoelectric clamped capacitance, v_p is the voltage across the piezoelectric element, and i_p is the current flowing through the element; α_e is the force–voltage factor of the piezoelectric element. The base acceleration $\ddot{y}(t)$, second derivative of the base displacement $y(t)$, is the mechanical excitation. Some literature discussed the energy harvesting under broad-band stochastic excitation [28], [29], while this paper only considers the harmonically excited case, i.e., $\ddot{y}(t)$ is purely sinusoidal. $x = z - y$ is the relative displacement. As far as the end devices are usually digital electronics, which require dc voltage power supply, an interface circuit is followed for ac–dc rectification. The device in Fig. 1 adopts the SEH interface circuit; a bridge rectifier is used for rectification, the filter capacitor $C_{\rm rect}$ acts as the energy storage, while $R_{\rm load}$ represents the dc load.

The dynamics of the SDOF representation can be described by

$$\begin{cases} M\ddot{x}(t) + D\dot{x}(t) + (K + K_p)\,x(t) + \alpha_e v_p(t) = -M\ddot{y}(t) \\ i_p(t) = \alpha_e \dot{x}(t) - C_p \dot{v}_p(t). \end{cases} \tag{1}$$

According to the electromechanical analogy

$$v_{\rm eq}(t) = -\frac{M}{\alpha_e}\ddot{y}(t) \tag{2}$$

$$i_{\rm eq}(t) = \alpha_e \dot{x}(t) \tag{3}$$

$$L = \frac{M}{\alpha_e^2} \tag{4}$$

$$R = \frac{D}{\alpha_e^2} \tag{5}$$

$$C = \frac{\alpha_e^2}{K + K_p} \tag{6}$$

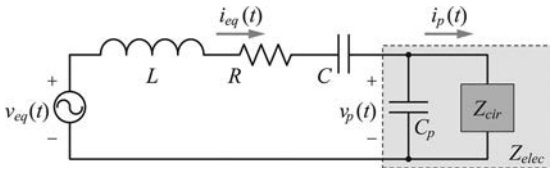

Fig. 2. Equivalent circuit of a base excited PEH device.

represent the equivalent voltage source, current, inductance, resistance, and capacitance, which correspond to the base excitation, relative velocity, mass, damping, and stiffness in the mechanical domain, respectively. Substituting the Fourier transforms of (2)–(6) into that of (1), we have

$$V_{\rm eq}\left(j\omega\right) = \left[j\omega L + R + \frac{1}{j\omega C} + Z_{\rm elec}\left(j\omega\right)\right] I_{\rm eq}\left(j\omega\right) \quad (7)$$

where ω is the excitation frequency, and

$$Z_{\rm elec}\left(j\omega\right) = \frac{V_p(j\omega)}{I_{\rm eq}(j\omega)} = \frac{1}{j\omega C_p} \| Z_{\rm cir}(j\omega) \quad (8)$$

represents the impedance of the electrical part.[1] The electrical part of the device is composed of C_p and the harvesting circuit, which are connected in parallel. The impedance of the connected harvesting circuit is

$$Z_{\rm cir}\left(j\omega\right) = \frac{V_p(j\omega)}{I_p(j\omega)} \quad (9)$$

Fig. 2 illustrates the equivalent circuit of the PEH device.

B. Impedance of the Electrical Part

In Section II-A, the electrical part of the PEH device was denoted as the impedance of $Z_{\rm elec}$. Yet, as we know, in the circuit analysis, the concept of impedance is usually used for linear ac circuits to show the magnitude and phase relations between voltage and current. So, strictly speaking, for all the ac–dc harvesting interfaces, even the simplest SEH, their behaviors cannot be completely described by the concept of impedance. Instead, we can only obtain the *equivalent impedance* of the electrical part for analysis. Approximation is made based on the assumption that the influence of higher order harmonics caused by the harvesting circuit to the system is much smaller than that of the fundamental harmonic. With this assumption, two simplified conditions are obtained.

1) The equivalent current $i_{\rm eq}$ can be regarded as perfect sine wave.
2) Only the fundamental harmonic of v_p, which is denoted as $v_{p,F}$, has an effect on the dynamic of the system.

Taking SEH for instance, given the equivalent current as

$$i_{\rm eq}(t) = I_0 \ \sin(\omega t) \quad (10)$$

where $I_0 = \alpha_e \omega X$ is the magnitude of $i_{\rm eq}(t)$, X is the magnitude of the relative displacement. The voltage across the piezoelectric element can be described by the following piecewise

[1]The notation '$\|$' represents the parallel connection of two components or networks. The impedance of $a\|b = (a^{-1} + b^{-1})^{-1}$.

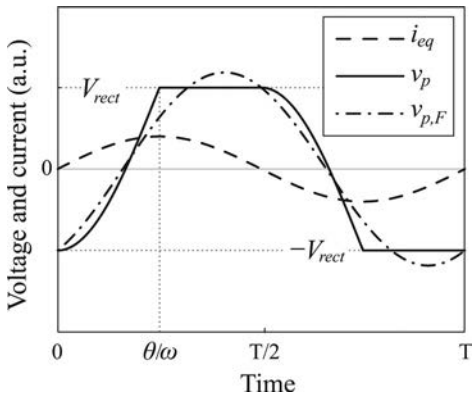

Fig. 3. Characteristic voltage and current waveforms in SEH.

equation:

$$v_p(t) = \begin{cases} V_{\rm oc}\left[1 - \cos(\omega t)\right] - V_{\rm rect}, & 0 \ \le \ \omega t < \theta \\ V_{\rm rect}, & \theta \ \le \ \omega t < \pi \\ V_{\rm rect} - V_{\rm oc}\left[1 + \cos(\omega t)\right], & \pi \ \le \ \omega t < \pi + \theta \\ -V_{\rm rect}, & \pi + \theta \ \le \ \omega t < 2\pi \end{cases} \quad (11)$$

where θ corresponds to the rectifier blocked angle in a half cycle (as illustrated in Fig. 3); $V_{\rm rect}$ is the rectified voltage; $V_{\rm oc}$ is the magnitude of the open circuit voltage

$$V_{\rm oc} = \frac{I_0}{\omega C_p} = \frac{\alpha_e X}{C_p}. \quad (12)$$

θ and $V_{\rm rect}$ are related by

$$\cos\theta = 1 - 2\tilde{V}_{\rm rect} \quad (13)$$

where $\tilde{V}_{\rm rect}$ is the nondimensional rectified voltage defined as

$$\tilde{V}_{\rm rect} = \frac{V_{\rm rect}}{V_{\rm oc}}. \quad (14)$$

The rectified voltage $V_{\rm rect}$ is the sum of $V_{\rm store}$ (the voltage across $C_{\rm rect}$) and V_F (the forward voltage drop of the bridge rectifier). According to (11), the expression on the fundamental harmonic of v_p is obtained as

$$v_{p,F}(t) = \frac{I_0}{2\pi\omega C_p}\left\{\left[\sin(2\theta) - 2\theta\right]\cos(\omega t) + 2\sin^2\theta\sin(\omega t)\right\}. \quad (15)$$

Under a specific value of $V_{\rm rect}$, Fig. 3 shows the waveforms of $i_{\rm eq}$, v_p, and $v_{p,F}$ in one vibration cycle. The equivalent impedance of the electrical part is obtained with the Fourier transforms of (10) and (15)

$$Z_{\rm elec}(j\omega) = \frac{V_{p,F}(j\omega)}{I_{\rm eq}(j\omega)} = \frac{1}{\pi\omega C_p}\left[\sin^2\theta + j\left(\sin\theta\cos\theta - \theta\right)\right]. \quad (16)$$

Since C_p in (16) is constant, $Z_{\rm elec}$ is a function of ω and θ. It is independent of the voltage source. The equivalent impedances

with other harvesting interface circuits can also be obtained with this method.

From the waveform point of view, distortion is observed by taking $v_{p,F}$ as the representation of v_p. But from the power point of view, given that $i_{\rm eq}$ is composed of a single harmonic and the fundamental component of $v_{p,F}$ is orthogonal to all high-order harmonics, the power consumed by $Z_{\rm elec}$ is calculated by

$$P_{\rm elec} = \frac{1}{T}\int_0^T v_p(t) i_{\rm eq}(t) {\rm d}t = \frac{1}{T}\int_0^T v_{p,F}(t) i_{\rm eq}(t) {\rm d}t. \quad (17)$$

Therefore, representing v_p with $v_{p,F}$ is reasonable for the power estimation within the dynamic PEH systems.

III. Investigations on the Electrical Part Impedance

Since the equivalent impedance of the electrical part $Z_{\rm elec}$ is composed of C_p and $Z_{\rm cir}$ connected in parallel, the equivalent impedance of the harvesting circuit $Z_{\rm cir}$ can be calculated as well. Previous studies on impedance matching [13]–[15] tended to regard $Z_{\rm cir}$ as the load impedance, while the output impedance of the transducer

$$Z_{\rm trans} = \frac{1}{j\omega C_p} \| \left[R + j\omega L + \frac{1}{j\omega C} \right] \quad (18)$$

as the source impedance. They assumed that the maximum power transfer can be achieved, when $Z_{\rm cir}$ matches $Z_{\rm trans}$. Yet, this viewpoint is inappropriate for two reasons: 1) The relation between the load and source impedances in the original impedance matching theory should be in series (with voltage source), or in parallel (with current source). But the relation between $Z_{\rm cir}$ and the transducer internal network is neither in series nor in parallel. 2) In the original impedance matching theory, the load impedance should be independent of the source impedance. But the $Z_{\rm cir}$ value in real PEH circuits cannot be specified without the knowledge about C_p.

On the contrary, in this paper, the piezoelectric capacitance C_p and the harvesting circuit are considered as a whole, i.e., the electrical part of the PEH system. Starting from this new viewpoint, it makes sure that the equivalent impedance network is a series network driven by a voltage source and the equivalent impedance $Z_{\rm elec}$ is independent of the rest impedances in the network. The definition of $Z_{\rm elec}$ was given in (16) by substituting v_p in (8) with $v_{p,F}$. In addition, different from the ordinary impedance, the attainable range and detailed composition of $Z_{\rm elec}$ require further investigation.

A. Range of the Electrical Part Impedance

The ranges of the electrical part equivalent impedance with four different interface circuits, including SEH, resistive shunt damping (RSD), P-SSHI, and S-SSHI, will be compared and discussed in this section. The interface circuit of SEH has been shown in Fig. 1, while those of RSD, P-SSHI, and S-SSHI are shown in Fig. 4.

In linear RSD, the electrical part is composed of C_p and $R_{\rm RSD}$ connected in parallel. Its impedance is

$$Z_{\rm elec}(j\omega) = \frac{1}{\omega C_p}\left(\frac{\rho}{1+\rho^2} - j\frac{\rho^2}{1+\rho^2}\right) \quad (19)$$

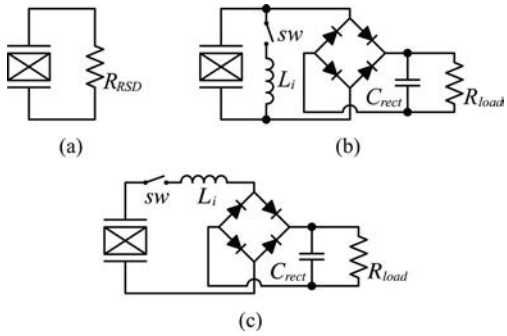

Fig. 4. Circuit topologies. (a) RSD. (b) P-SSHI. (c) S-SSHI.

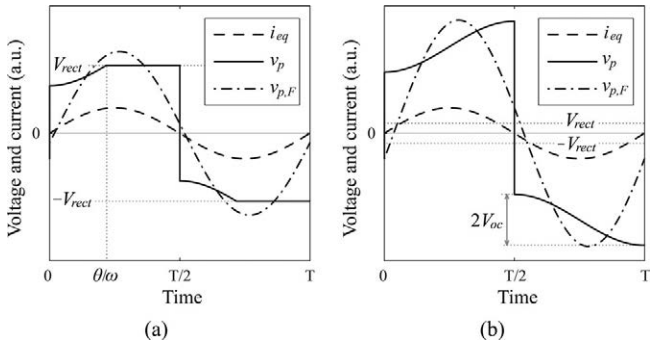

Fig. 5. Characteristic voltage and current waveforms in the SSHI interface circuits. (a) P-SSHI. (b) S-SSHI.

where

$$\rho = \omega C_p R_{\rm RSD} \quad (20)$$

is the nondimensional shunt resistance in RSD.

The SSHI interface circuit is constructed by adding a synchronized switching path to the SEH one. By taking the switching actions once the displacement x reaches its extreme values, it intervenes in the transduction process in a semipassive way, so as to increase the harvested power. The detailed principles and advantages of P-SSHI and S-SSHI have been investigated [6], [7], [11], [30], [31]. The waveforms of i_{eq}, v_p, and $v_{p,F}$ in P-SSHI and S-SSHI are shown in Fig. 5. With the same method for SEH, which was given in Section II-B, the equivalent impedances of the electrical parts in P-SSHI and S-SSHI can also be studied. In SSHI, since the switching interval for voltage inversion is usually chosen much shorter than the mechanical cycle, the voltage inversion is regarded to be finished in an instant. For P-SSHI, the voltage across the piezoelectric element is expressed with the following piecewise equation:

$$v_p(t) = \begin{cases} V_{\rm oc}\left[1-\cos(\omega t)\right] - \gamma V_{\rm rect}, & 0^+ \ \le\ \omega t < \theta \\ V_{\rm rect}, & \theta \ \le\ \omega t \le \pi^- \\ \gamma V_{\rm rect} - V_{\rm oc}\left[1+\cos(\omega t)\right], & \pi^+ \ \le\ \omega t < \pi+\theta \\ -V_{\rm rect}, & \pi+\theta \ \le\ \omega t \le 2\pi^- \end{cases} \quad (21)$$

where γ is the voltage inversion factor in every switching action. It was defined as the voltage ratio after and before the voltage inversion, and related to the quality factor Q of the switching

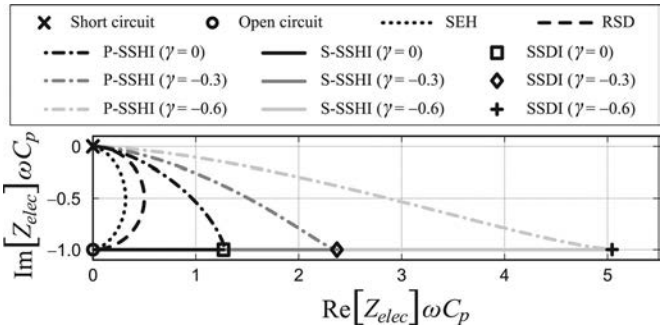

Fig. 6. Electrical part equivalent impedance with four different interface circuits (nondimensionalized with $(\omega C_p)^{-1}$, the impedance magnitude under open circuit condition).

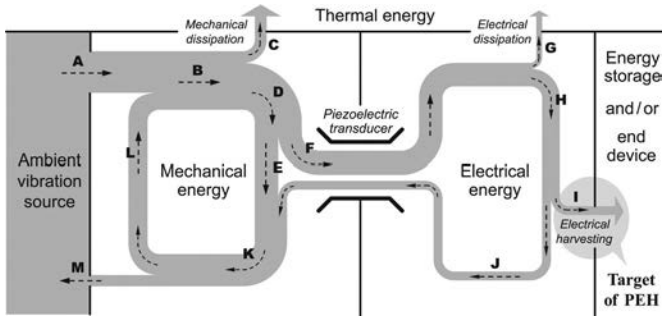

Fig. 7. Energy flow chart of a base excited PEH device.

$C_p - L_i - r$ loop (r is the parasitic resistance in the loop) with the following relation [11]:

$$\gamma = -e^{-\pi/(2Q)}. \tag{22}$$

The fundamental harmonic of v_p in P-SSHI can be calculated with (21). Accordingly, the equivalent impedance of the electrical part is obtained as

$$Z_{\rm elec}(j\omega) = \frac{1}{\pi\omega C_p}\left[(1-\cos\theta)\left(\frac{4}{1+\gamma} - 1 + \cos\theta\right) + j\left(\sin\theta\cos\theta - \theta\right)\right]. \tag{23}$$

Different from SEH, in P-SSHI, θ and $V_{\rm rect}$ are related by

$$\cos\theta = 1 - (1+\gamma)\tilde{V}_{\rm rect}. \tag{24}$$

In S-SSHI, the voltage across the piezoelectric element is

$$v_p(t) = \begin{cases} -V_{\rm oc}\cos(\omega t) + \frac{1-\gamma}{1+\gamma}(V_{\rm oc} - V_{\rm rect}), & 0^+ \le \omega t \le \pi^- \\ -V_{\rm oc}\cos(\omega t) - \frac{1-\gamma}{1+\gamma}(V_{\rm oc} - V_{\rm rect}), & \pi^+ \le \omega t \le 2\pi^-. \end{cases} \tag{25}$$

The corresponding electrical part equivalent impedance is obtained as

$$Z_{\rm elec}(j\omega) = \frac{1}{\omega C_p}\left[\frac{4}{\pi}\frac{1-\gamma}{1+\gamma}(1-\tilde{V}_{\rm rect}) - j\right]. \tag{26}$$

As observed from (26), the imaginary component of $Z_{\rm elec}$ in S-SSHI is constant and equals the impedance under open circuit condition, i.e., $(j\omega C_p)^{-1}$.

According to (16), (19), (23), and (26), Fig. 6 shows the electrical part equivalent impedances with the four different interface circuits on the complex impedance plane, which is nondimensionalized with $(\omega C_p)^{-1}$, i.e., the impedance magnitude under open circuit condition. Only the points on the corresponding curve are attainable for a specific interface circuit. Therefore, the attainable impedance range is constrained, rather than able to be arbitrarily set. This makes the harvested power optimization in PEH systems different from the conventional unconstrained impedance matching.

Comparisons between SEH and RSD have been made [11], [13], [15], [32]. It has been shown that the performances of SEH and RSD are different; the ratio between their maximum extractable powers is $2/\pi$. From Fig. 6, the impedance ranges of SEH and RSD are not overlapped except for the points corresponding to short and open circuits; therefore, their responses to the same excitation are again shown to be different. The real component of the equivalent impedance is related to the extracted power. In a general matching case, it is not necessary that the larger the real component, the more the power delivered. But in weakly coupled systems, the equivalent resistance in the mechanical part, i.e., R in Fig. 2, is much larger than the real component of $Z_{\rm elec}$. Under this condition, the larger the real component, the more the power delivered to the electrical part. Therefore, the maximum extractable power of RSD is larger than SEH. Both P-SSHI and S-SSHI can greatly increase the real component of the equivalent impedance (the smaller the inversion factor γ, the larger the increase on the real component); therefore, the extracted power can be further increased by P-SSHI and S-SSHI. In addition, under the same inversion factor γ, the curves of P-SSHI and S-SSHI converge at a point, where the real parts of their electrical part equivalent impedances are maximized. This point corresponds to the case of synchronized switch damping on inductor [33] under the same γ.

B. Energy Flow

The objective of impedance matching for a general system is to maximize the power delivered to the load. But for the energy harvesting systems, the objective is vague. Various researchers have made conflicting claims [16]. The reason is attributed to the ambiguous understanding on the concept of *load* in energy harvesting. In a conventional system, load consumes all the power that is extracted from the system. Whereas, in a harvesting system, the concern is how much energy is scavenged and/or used to power the end device rather than directly consumed. The harvested energy is only one portion of the extracted energy. The clarification on energy flow helps straighten out the detailed composition in $Z_{\rm elec}$, so that the objective of harvested power optimization in energy harvesting systems can be further identified.

Liang and Liao compared the energy flow among three different piezoelectric devices and clarified that the functions of energy harvesting and energy dissipation are coexistent in a harvesting interface circuit [12]. Both of them bring out structural damping [11]. The energy flow within a base excited PEH

device is shown in Fig. 7. The energy flow chart provides an intuitive way to indicate the directions of different branches of flow in every vibration cycle. In the electrical domain, with different interface circuits connected, this electrical energy may have different destinations. Generally, there are three possible ways:

1) being converted into thermal energy (branch G), i.e., dissipated;
2) being stored in energy storage devices and/or used to power the end device (branch I), i.e., harvested;
3) returning to the mechanical domain (branch J).

While taking the electrical part as an equivalent impedance, its real component always absorbs energy without any return; on the other hand, its imaginary component alternately absorbs energy from the system and then all returns. Comparing the two components in the electrical part equivalent impedance and the aforementioned three items, the imaginary component corresponds to item 3; while the real component contributes to the total effect of items 1 and 2. Among the three items, only item 2, i.e., the harvested power, is the target of energy harvesting, as highlighted in Fig. 7.

The distinction between the extracted power and harvested power was not clear in some of the previous literature [9], [10], in particular those studies, which adopted resistive equivalence for the harvesting circuit [19], [20]. The detailed investigation on energy flow helps identify the target of power optimization between these two branches. In addition, studies showed that the harvested power is not proportional to the extracted power in the existing harvesting interface circuits [12], [34]. So even $Z_{\rm elec}$ matches the equivalent impedance of the mechanical part, which implies that the extracted power is maximized, there is no guarantee that the harvested power is optimized.

IV. Equivalent Electrical or Mechanical Models

Based on the detailed investigation about the electrical part equivalent impedance within the PEH system, the effects of different harvesting interface circuits on system dynamics were better understood, in terms of impedance. The dynamics of a PEH system can now be described by an equivalent model in either fully electrical or fully mechanical domain.

A. Equivalent Impedance Network

In the equivalent circuit shown in Fig. 2, the effect of the electrical part was regarded as a whole, i.e., represented by $Z_{\rm elec}$. To further figure out its contributions corresponding to the three branches of energy flow in the electrical part, $Z_{\rm elec}$ can be further divided into three components connected in series: *vibratory component* X_E, *harvesting component* R_h, and *dissipative component* R_d. Since the total extracted power is the sum of the harvested and dissipated power, the real component of $Z_{\rm elec}$ is composed of R_h and R_d. The imaginary component of $Z_{\rm elec}$ corresponds to the vibratory component X_E. Fig. 8 shows the equivalent impedance network of a PEH device. The real components are represented by gray blocks, while the imaginary ones are represented by white blocks. X_L and X_C are the corresponding reactances of L and C, respectively. From the

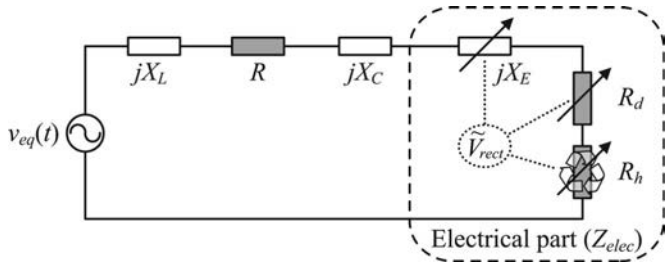

Fig. 8. Equivalent impedance network of a base excited PEH device.

viewpoint of the excitation source, all of R_h, R_d, and R absorb energy from the source, whereas their functions are different. Therefore, in Fig. 8, R_h is distinguished with a "recycling" mark. As illustrated in Fig. 6, the impedance of an interface circuit is adjustable, but unable to be arbitrarily set. The components of R_d, R_h, and X_E are variables (denoted with arrows) as functions of the nondimensional rectified voltage $\tilde{V}_{\rm rect}$ (illustrated with dot lines linking to $\tilde{V}_{\rm rect}$). Since the ratio between R_d and R_h under specific rectified voltage $\tilde{V}_{\rm rect}$ can be obtained through an energy cycle analysis [11], [12], together with the expression of $Z_{\rm elec}$, the values of R_d, R_h, and X_E can be calculated.

The dissipative component R_d in the SEH interface is attributed to the forward voltage drop of the rectifier, i.e., V_F. In SEH

$$R_d = \frac{4}{\pi\omega C_p}\tilde{V}_F(1-\tilde{V}_{\rm rect}) \tag{27}$$

$$R_h = \frac{4}{\pi\omega C_p}(\tilde{V}_{\rm rect}-\tilde{V}_F)(1-\tilde{V}_{\rm rect}) \tag{28}$$

$$X_E = \frac{1}{\pi\omega C_p}\left(\sin\theta\cos\theta-\theta\right) \tag{29}$$

where $\tilde{V}_F$ is the nondimensional forward voltage drop defined as

$$\tilde{V}_F = \frac{V_F}{V_{\rm oc}}. \tag{30}$$

For P-SSHI and S-SSHI, the dissipative component R_d is composed of the rectifier dissipation and the dissipation produced during the switching actions. In P-SSHI

$$R_d = \frac{1}{\pi\omega C_p}\{2\tilde{V}_F[2-\tilde{V}_{\rm rect}(1+\gamma)]+\tilde{V}_{\rm rect}^2(1-\gamma^2)\} \tag{31}$$

$$R_h = \frac{2}{\pi\omega C_p}(\tilde{V}_{\rm rect}-\tilde{V}_F)\left[2-\tilde{V}_{\rm rect}(1+\gamma)\right] \tag{32}$$

$$X_E = \frac{1}{\pi\omega C_p}\left(\sin\theta\cos\theta-\theta\right). \tag{33}$$

In S-SSHI,

$$R_d = \frac{4}{\pi\omega C_p}\frac{1-\gamma}{1+\gamma}(1-\tilde{V}_{\rm rect}+\tilde{V}_F)(1-\tilde{V}_{\rm rect}) \tag{34}$$

$$R_h = \frac{4}{\pi\omega C_p}\frac{1-\gamma}{1+\gamma}(\tilde{V}_{\rm rect}-\tilde{V}_F)(1-\tilde{V}_{\rm rect}) \tag{35}$$

$$X_E = -\frac{1}{\omega C_p}. \tag{36}$$

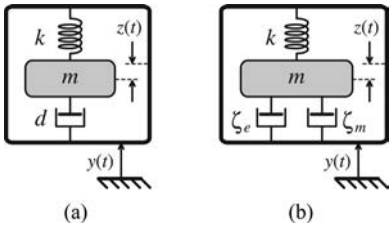

Fig. 9. Early equivalent mechanical schematics of a base excited PEH device. (a) Model proposed by Williams and Yates [35]. (b) Revision by Hudak and Amatucci [37].

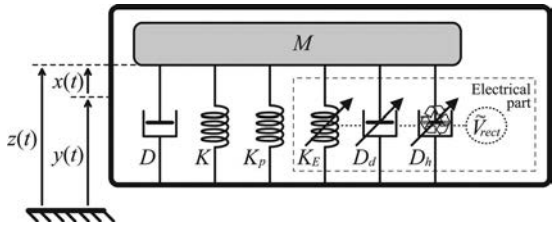

Fig. 10. Equivalent mechanical schematics of a base excited PEH device.

As observed from (29) and (33), X_E are the same in SEH and P-SSHI under the same θ. The parameter θ in these two cases was defined in (13) and (24), respectively; SEH can be regarded as a special case of P-SSHI, in which the inversion factor $\gamma = 1$.

B. Equivalent Mechanical Schematics

For the fully equivalent mechanical modeling, one widely referred model for vibration energy harvesting was proposed by Williams and Yates [35] as shown in Fig. 9(a). In their model, the effect of energy harvesting toward the structural dynamics was reflected by its induced damping, i.e., illustrated with the dashpot d in Fig. 9(a). They have also considered the effect of the so-called "unwanted damping" in the system, but it was not shown in their schematics. Ever since then, most literature, including a majority of review articles [5], [36]–[40], regarded this model as the general model for vibration energy harvesting devices, including piezoelectric, electromagnetic, and electrostatic. Hudak and Amatucci [37] further specified the role of the "unwanted damping." As shown in Fig. 9(b), in their revised model, the harvesting induced damping was represented by the electrical damping ratio ζ_e; the "unwanted damping" mentioned in [35] was represented by the mechanical damping ratio ζ_m.

Yet, in the PEH research, Erturk and Inman [41] pointed out that the backward coupling effect from electrical to mechanical domain cannot be simply represented by only electrically induced damping; therefore, the expression on harvested power given in [35] needed to be revised for PEH. Nevertheless, in their study, the entire harvesting circuit was represented by a linear shunt resistor; therefore, the system that they have considered in fact was an RSD system. In some literature, in particular those emphasizing on the mechanical part, RSD was used for the harvested power estimation. From the research point of view, it is understandable, in particular, when the mechanical model is complicated. However, from the practical point of view, Mitcheson *et al.* [38] pointed out that a pure resistive ac load is not useful and a typical load will be a diode rectifier and smoothing capacitor, i.e., an SEH interface. Therefore, to investigate the dynamics as well as the optimal harvested power in real harvesting interfaces is of importance in many practical applications [30], [31], [42].

The dynamics of a PEH system with real harvesting interface circuits, e.g., SEH, P-SSHI, or S-SSHI would be more complicated than what was presented in Williams and Yates's model, and might also be different from what Erturk and Inman have shown with the RSD equivalence for the PEH system. It can be investigated with the impedance modeling and analysis proposed in this paper. Referring to the mechanical to electrical analogies given by (4)–(6), which were used to obtain the equivalent electrical components L, R, and C from the corresponding mechanical components M, D, and $K + K_p$, the three impedance components in $Z_{\rm elec}$, i.e., R_d, R_h, and X_E, shown in Fig. 8, can be inversely converted into equivalent dissipative dashpot D_d, regenerative dashpot D_h, and electrical induced stiffness K_E with the following relations:

$$D_d = \alpha_e^2 R_d \tag{37}$$

$$D_h = \alpha_e^2 R_h \tag{38}$$

$$K_E = -\alpha_e^2 \omega X_E. \tag{39}$$

As observed from Fig. 6, in the harvesting interface circuits discussed in this paper, X_E are all negative; therefore, the equivalent K_E is positive in these interfaces. D_d, D_h, and K_E are variables and change with the nondimensional rectified voltage $\tilde{V}_{\rm rect}$. They reflect the three coexistent functions in the electrical part of a real harvesting interface circuit.

Fig. 10 illustrates the equivalent mechanical schematics, which corresponds to the equivalent impedance network shown in Fig. 8. Compared to the extensively referred models in Fig. 9 [35], [37], it shows that the backward coupling effect caused by the connected circuits cannot be reflected by merely the damping effect. Compared to the analysis by Erturk and Inman [41], it reveals the different functional compositions within a real harvesting circuit, which is necessary for the identification on the objective of PEH optimization.

V. Harvested and Extracted Powers

As mentioned earlier, in the design of PEH devices, the extracted power could be confused with the harvested power. In some literature [9], [10], [19], [20], the extracted power was wrongly taken as the optimization objective. From the energy flow chart given in Fig. 7, the relation between these two branches of energy flow were clarified. In the equivalent impedance network shown in Fig. 8, different functions were reflected by their corresponding components, respectively. With these analyses, it is intelligible to identify the harvested power, i.e., the power delivered to the harvesting component R_h, as the optimization objective. Comparing of the equivalent impedance network here to the general impedance network, R_h should be regarded as the "load impedance," while the other components in series form the "source impedance." Fig. 11 illustrates the

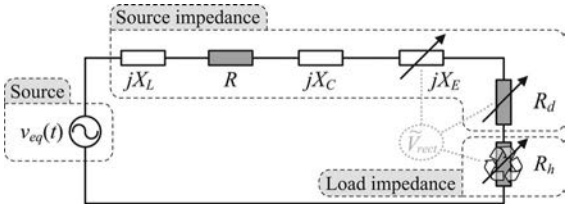

Fig. 11. Identification of different components in the equivalent impedance network.

identification of different components in the equivalent impedance network.

In the matching of a general impedance network, the source impedance is fixed. If the load impedance is an arbitrary complex number, the maximum load power is attained, when the load impedance is the complex conjugate of the source impedance, i.e.,

$$Z_{\text{load}} = Z^*_{\text{source}}. \tag{40}$$

If the load impedance is an arbitrary real number, i.e., resistive load, the load power is maximized when the load impedance equals the magnitude of the source impedance, i.e.,

$$Z_{\text{load}} = |Z_{\text{source}}|\,. \tag{41}$$

Yet, for the equivalent impedance network of a PEH system shown in Fig. 11, both (40) and (41) are not applicable. Because there are two differences between this network and those discussed for conversional complex or resistive impedance matching.

1) The source impedance is also variable. It changes in company with the load impedance.
2) The load impedance R_h is purely resistive; yet, it is constrained, rather than arbitrary.

Even the conventional impedance matching theory is not applicable to the PEH system, the harvested power can still be obtained with the impedance-based analysis as

$$P_h = \frac{V_{\text{eq}}^2}{2}\frac{R_h}{(X_L + X_C + X_E)^2 + (R + R_d + R_h)^2} \tag{42}$$

where V_{eq} is the magnitude of the equivalent voltage source $v_{\text{eq}}(t)$, which is constant for the base excited case. The electrically extracted power is given as

$$P_\Delta = \frac{V_{\text{eq}}^2}{2}\frac{R_h + R_d}{(X_L + X_C + X_E)^2 + (R + R_d + R_h)^2}. \tag{43}$$

P_h and P_Δ are functions of ω and $\tilde{V}_{\text{rect}}$. When the excitation frequency ω is determined, the maximum P_h is theoretically obtained at the zero derivative point, i.e., $\partial P_h/\partial \tilde{V}_{\text{rect}} = 0$. Closed-form expression on the optimum $\tilde{V}_{\text{rect}}$ is preferred; however, the transcendental equation is unable to be solved with an analytical method. It is solvable with the numerical method; it seems more convenient to obtain the optimum by substituting the expressions of R_h, R_d, and X_E into (42) and numerically searching for the maximum P_h under different $\tilde{V}_{\text{rect}}$.

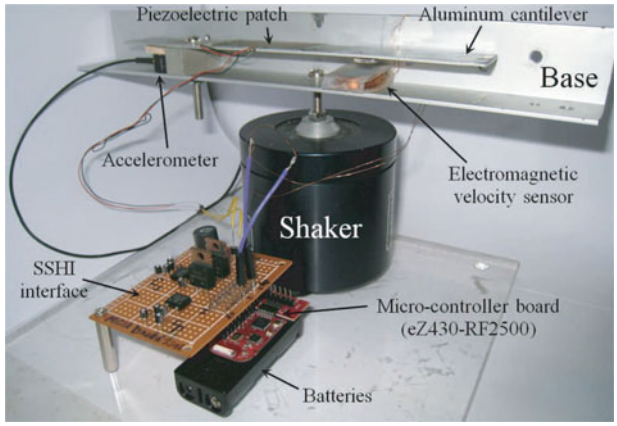

Fig. 12. Experimental setup of a base excited PEH device.

VI. Experiments

Experiments are carried out with a base excited piezoelectric energy harvester for three cases. In each case, one of the interface circuits among SEH, P-SSHI, and S-SSHI is connected to the piezoelectric cantilever. The harvested power is theoretically obtained as functions of $\tilde{V}_{\text{rect}}$. The actual harvested power is experimentally measured for comparison.

A. Experimental Setup

Fig. 12 shows the experimental setup. The main mechanical structure is an aluminum cantilever, whose excitation is from a shaker (4810, Brüel and Kjær, Denmark). A piezoceramic patch of 49 mm $\times$ 24 mm $\times$ 0.508 mm (T120-A4E-602, Piezo System, Inc., Woburn, MA) is bonded near the fixed end. An accelerometer (4501, Brüel and Kjær, Denmark) is installed at the fixed end to track the base acceleration. For the purpose of synchronization in both P-SSHI and S-SSHI, an electromagnetic sensor is employed to sense the relative velocity between the cantilever beam and the base. The permanent magnet acts as a proof mass at the same time. It can lower the natural frequencies and increase the displacement at the free end. The output voltage from the coil, which is proportional to the end velocity, is then input to a microcontroller unit (eZ430-RF2500, Texas Instrument, Dallas, TX). In the circuit part, the microcontroller is coded to first analyze the velocity signal, and then generate switching commands to drive the MOSFET switch for performing synchronized switching actions.

B. Parameters Identification

In this study, the parameters of the piezoelectric structure are identified from measurement. Disconnecting the excitation v_{eq} and the connected harvesting interface circuit Z_{cir} from the equivalent circuit in Fig. 2, we obtained the configuration of the internal impedance of the free piezoelectric structure. It was also known as Van Dyke's model [43], as shown in

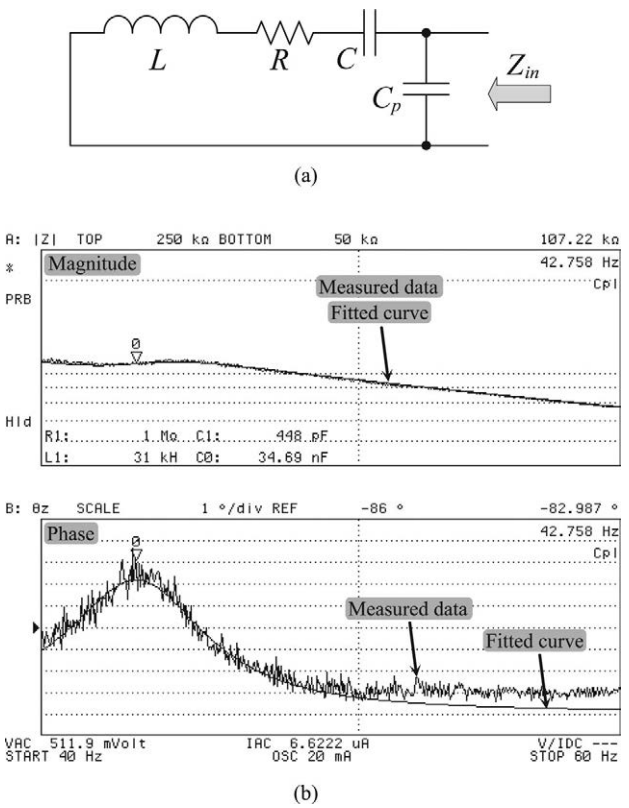

Fig. 13. Internal impedance of the piezoelectric structure. (a) Van Dyke's model. (b) Measured and fitted results.

Fig. 13(a). The measured result of the internal impedance is obtained with an impedance analyzer (4294A, Agilent, Santa Clara, CA), and is shown in Fig. 13(b). The values of different components in Van Dyke's model are obtained by fitting the experimental waveforms. The fitted curves are also shown in Fig. 13(b); the values of L, R, C, and C_p are listed in Table I. The short-circuit natural frequency f_0 is about 42.76 Hz. The force–voltage factor α_e can be indirectly obtained from the measured results. Badel *et al.* [24] derived α_e based on the relation that was given in (12). In (12), the clamped capacitance C_p can be measured with the clamped piezoelectric structure; the magnitude of the open circuit voltage $V_{\rm oc}$ can be observed with an oscilloscope; yet, X was taken as the tip displacement magnitude of the cantilevered structure. But precisely speaking, since the SDOF approximation of the one-end-fixed cantilevered structure was used in [24], the parameter X should correspond to the displacement magnitude of the *equivalent mass* in the SDOF representation. Nevertheless, the center of the equivalent mass is not easy to be positioned for displacement measurement.

On the other hand, in this paper, we derive α_e with the base excited piezoelectric cantilevered structure. Assuming that, when the applied harmonic base acceleration is at the magnitude of $\ddot{Y}$ (measured with the accelerometer embedded in the base), the magnitude of the open circuit voltage without circuit connected is measured as $V_{\rm oc}$. The equivalent voltage source $V_{\rm eq}$ can be estimated with the following relation:

$$V_{\rm eq} = \frac{|R + j(X_L + X_C + X_{Cp})|}{|jX_{Cp}|} V_{\rm oc} \tag{44}$$

where X_{Cp} is the reactance of the clamped capacitance C_p. Substituting the values of $V_{\rm eq}$ and $\ddot{Y}$ into (2) gives the value of M/α_e. Since the value of L was known, substituting M/α_e into (4) yields the value of α_e.

Platt *et al.* [25] proposed another experimental method for identifying parameters by fitting the relation between the input force and output voltage across the piezoelectric element. But the data on force and voltage need to be measured one by one; it is not as efficient as that utilizing the impedance analyzer for parameter identification.

The parameters of the interface circuit in the experimental setup are listed in Table I.

TABLE I
PARAMETERS OF THE EXPERIMENTAL SETUP

Component	Value or model
L	31 kH
R	1 MΩ
C	448 pF
C_p	34.69 nF
f_0	42.76 Hz
α_e	4.75×10^{-4} N/V
sw	MOSFET (IRL510)
Rectifier	DB104 ($V_F = 1.0$ V)
γ	-0.7
L_i	47 mH
C_{rect}	1, 10, 22 μF

C. Results

Given a 42 Hz and 10 m/s^2 (in rms) harmonic base excitation, the harvested power for different $\tilde{V}_{\rm rect}$ is studied both theoretically and experimentally. Experiments are carried out to obtain the P_h under different $\tilde{V}_{\rm rect}$. In experiments, different dc load resistors $R_{\rm load}$ are connected one after another to stabilize the $V_{\rm store}$ at different levels. The corresponding experimental P_h is obtained with

$$P_{h,\rm exp} = \frac{V_{\rm store}^2}{R_{\rm load}}. \tag{45}$$

For the measurement of $\tilde{V}_{\rm rect}$, $V_{\rm rect}$ is the sum of $V_{\rm store}$ and V_F (1.0 V for the bridge rectifier we used), but $V_{\rm oc}$ changes under different $V_{\rm rect}$. It is better to take the rectifier blocked interval θ/ω as the direct measured parameter in SEH and P-SSHI, as illustrated by Figs. 3 and 5(a),[2] and then obtain $\tilde{V}_{\rm rect}$ with (13) and (24), respectively. And for S-SSHI, there is no rectifier blocked angle θ, but $2V_{\rm oc}$ can be directly measured from the waveform, as illustrated in Fig. 5(b).

The theoretical and experimental results on the harvested power are shown in Fig. 14 for comparison. The theoretical

[2]In the practical implementation of P-SSHI, as there is a reversion after every voltage inversion [44], θ/ω should be the time interval started at the lowest point after the reversion and ended when the bridge rectifier is conducted.

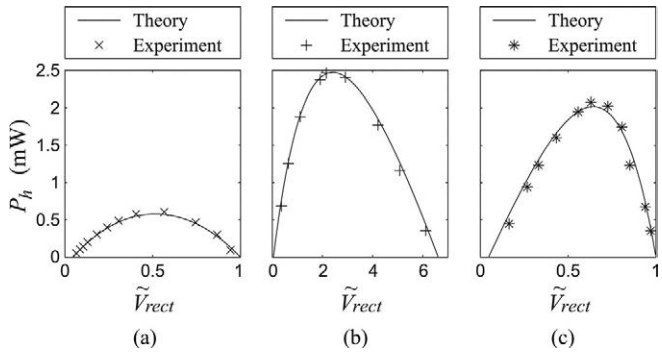

Fig. 14. Theoretical and experimental results on the harvested power with different interface circuits. (a) SEH. (b) P-SSHI. (c) S-SSHI.

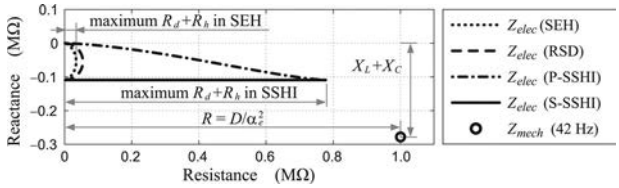

Fig. 15. Mechanical and electrical impedances in the experiments.

results match the experimental data very well. The P-SSHI provides the maximum harvestable power among the three cases. For this specific based excited PEH device, the improvements of implementing P-SSHI and S-SSHI, compared to SEH, are about 500% and 400%, respectively. The improvement in implementing these two interfaces, yet, might be different between two different devices, since they also depend on the mechanical characteristics. The maximum power under each condition can be obtained from the corresponding numerical result.

Previous studies on P-SSHI and S-SSHI were mostly conducted under constant displacement excitation [24], [45]. Under constant displacement excitation, the P_h curve is symmetric with the middle value in the $\tilde{V}_{\rm rect}$ range for all the SEH, P-SSHI, and S-SSHI interface circuits [24]. Yet, from Fig. 14, the shapes are asymmetric, in particular, for P-SSHI and S-SSHI. The SEH curve seems still symmetric. The reason is that its $Z_{\rm elec}$ is far from the equivalent impedance of the mechanical part in this device; therefore, harvesting with this interface circuit makes little influence on the system dynamics. The displacement of this device changes little with the SEH interface circuit. In general, the optimum rectified voltage differs under constant displacement and constant force excitations; ignoring the difference might lead to error in the harvested power optimization.

Fig. 15 shows the equivalent impedance of both mechanical and electrical parts in the experiments. Their real components correspond to R and $R_d + R_h$, respectively. It can be observed that both the P-SSHI and S-SSHI can greatly extend the real component of $Z_{\rm elec}$, compared to RSD and SEH. However, in this case, the $R_d + R_h$ still cannot catch up with R. The ratio between $R_d + R_h$ and R can be increased by three means:

1) implement more sophisticated circuit, so as to increase $R_h + R_d$, e.g., replace SEH with P-SSHI or S-SSHI; or decrease the voltage inversion factor γ in the SSHI circuits;
2) decrease the inherent mechanical damping D;
3) increase the force–voltage factor α_e.

These three means imply that all the electrical circuit, mechanical structure, and transducer can shorten the distance between $R_d + R_h$ and R, and therefore increase the power extraction.

Besides, as mentioned in Section III, the previous literature [13]–[15] assumed that maximum power transfer can be achieved, when $Z_{\rm cir}$, the input impedance of the harvesting circuit, matches $Z_{\rm trans}$, the output impedance of the transducer. Based on this concept, the "matched" $Z_{\rm cir}$ is $Z^*_{\rm trans}$ in the complex conjugate matching, and is $|Z_{\rm trans}|$ in the resistive matching. Given the values of the internal components of L, R, C, and C_p in Table I, in the complex conjugate matching case, the "matched" $Z_{\rm cir}$ is calculated to be $(10.4 + 105.2i)$ kΩ; the corresponding extracted power is 5.4 mW. In the resistive matching case, the "matched" $Z_{\rm cir}$ is calculated to be 105.7 kΩ; the corresponding extracted power is 0.97 mW. Comparing these two results to those given in Fig. 14, neither of them can reflect the harvested power in the PEH systems with real harvesting circuits, not to mention that the extracted power and harvested power even cannot be distinguished with the transducer and harvesting circuit matching concept.

VII. Discussion

Previous analyses on the harvested power in the PEH systems can be classified into three categories. Early analyses modeled the piezoelectric structure as an ideal current source in parallel with the piezoelectric capacitance [10], [32], [46], [47]. These analyses were valid under constant displacement excitation, or force excitation with the uncoupled assumption. Guyomar *et al.* [6], [7] suggested a power analysis under constant force excitation; but in fact, the force magnitude is only used to determine the displacement level at the presumed "optimum point," where the excitation force and vibration velocity are in phase. Shu *et al.* pointed out the insufficiencies of both the uncoupled and inphase analyses under constant force excitation. They further provided the improved analyses for the PEH devices with the SEH [42], P-SSHI [30], and S-SSHI [31] interface circuits.

The impedance-based analysis proposed in this paper shares some common features with Shu *et al.'s* studies. However, the underlying concepts are different. They used the energy balance analysis; we considered the fundamental harmonic. The methodologies are different too. Shu *et al.* started the solution from the viewpoint of overall dynamics; we took the bottom up approach by analyzing the dynamic characteristics of every component first. The relation between Shu *et al.'s* solution and ours is similar to the ac circuit analyses with differential equations and the impedance approach. Both methods are valuable but not exclusive.

To compare with Shu *et al.'s* result, the explicit expression on the normalized harvested power is also calculated with our approach by omitting the dissipated power caused by the

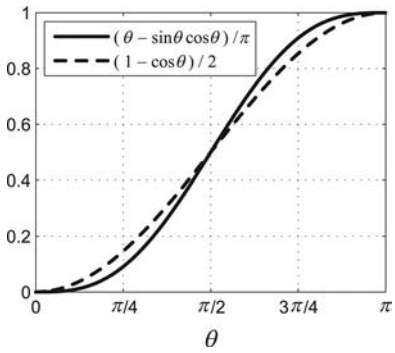

Fig. 16. Comparison of two functions of θ.

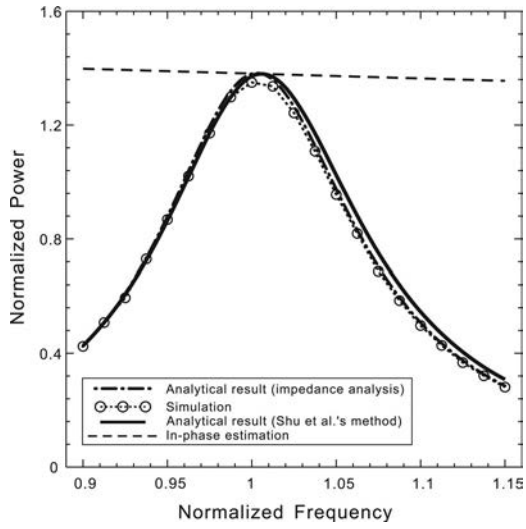

Fig. 17. Normalized harvested power compared to Shu *et al.*'s result [30].

rectifier. For the S-SSHI case, the explicit expressions obtained with the two approaches are exactly the same. For the SEH and P-SSHI cases, with the both approaches, the normalized harvested power is expressed as follows:

$$\bar{P}_h = \frac{\omega_{sc}}{M\ddot{Y}^2}P_h = \frac{\frac{4k_e^2\Omega^2 r}{[\pi+(1-q_1)r\Omega]^2}}{\left\{2\zeta_m + \frac{4k_e^2 r\left[2+\frac{r\Omega}{\pi}(1-q_1^2)\right]}{[\pi+(1-q_1)r\Omega]^2}\right\}^2\Omega^2 + [1-\Omega^2+k_e^2 A]^2} \tag{46}$$

where the parameters ω_{sc}, k_e^2, Ω, r, q_1, and ζ_m follow the definition in [30], [42], and [31].[3] The difference lies on the variable A in (46). With the impedance analysis proposed in this paper

$$A = \frac{\theta - \sin\theta\cos\theta}{\pi} \tag{47}$$

while with Shu *et al.*'s approach

$$A = \frac{1-\cos\theta}{2}. \tag{48}$$

[3]The parameters of α_e, D, $K+K_p$, R_{load} and γ in our derivation correspond to Θ, η_m, K, R, and $-q_1$ in [30], [31], and [42].

The parameter θ here uses the definition given by (24), rather than that given in [30], [42], and [31]. Since the range of θ is $[0,\ \pi]$, plotting the two functions of (47) and (48) in Fig. 16, we can find they are close within this range. The difference is generally caused by the different approaches used in the two analyses. In order to compare with Shu *et al.*'s result in [30], using the same parameters, we plot the analytical result obtained with the impedance approach in the same figure that was given in their paper, as shown in Fig. 17. It is shown that the two analytical results are very close; compared to Shu *et al's* analytical result, the result obtained with the impedance analysis gives even better approximation to the simulation result in the high-frequency range.

Based on the comparison, the similarities and differences between the two approaches are clarified. Both of them can be used to analyze the dynamics and harvested power in the PEH systems with real harvesting circuits. Meanwhile, the impedance analysis gives more insights on the detailed configuration of the PEH systems. It enables the application of the conventional ac power analysis in the PEH systems.

VIII. Conclusion

The impedance matching theory is useful in load power optimization. Yet, for the research on PEH, several issues should be addressed before utilizing the impedance concept for harvested power optimization. The methodologies to obtain the equivalent impedances of the mechanical and electrical parts were proposed. Only when both sides are uniformly modeled in terms of impedance, the utilization of the impedance method to study the dynamics of an entire PEH system can be realized. Moreover, we studied the constraints on the electrical part equivalent impedances corresponding to three different interface circuits, including SEH, P-SSHI, and S-SSHI. Since there is only one tunable parameter in either of these interface circuits, the range of the electrical equivalent impedance is constrained on a specific curve, rather than able to be arbitrarily set in the complex impedance plane, as claimed in some literature. Considering the energy flow within the PEH system, the objective of harvested power optimization was clarified in terms of impedance. This understanding is also valuable for the harvested power optimization in other energy harvesting technologies. According to these two issues in the electrical part, which were ignored in the previous studies, the equivalent impedance network and equivalent mechanical schematics of a PEH system were proposed and discussed.

It has been shown that the harvested power optimization procedures for PEH systems are different from the general impedance matching approaches. In these PEH cases, both the load and source impedances are dependent variables. Moreover, their values are constrained, rather than can be arbitrarily set. Taking these into consideration, the power optimization was carried out with the numerical method in our analysis. Experiments showed that the impedance-based analysis can model the dynamics of a base excited PEH system and well predict the maximum harvested power.

REFERENCES

[1] W. H. Liao, D. H. Wang, and S. L. Huang, "Wireless monitoring of cable tension of cable-stayed bridges using PVDF piezoelectric films," *J. Intell. Mater. Syst. Struct.*, vol. 12, no. 5, pp. 331–339, 2001.

[2] W. Wang and O. A. Jianu, "A smart sensing unit for vibration measurement and monitoring," *IEEE/ASME Trans. Mechatronics*, vol. 15, no. 1, pp. 70–78, Feb. 2010.

[3] K. Kong and M. Tomizuka, "A gait monitoring system based on air pressure sensors embedded in a shoe," *IEEE/ASME Trans. Mechatronics*, vol. 14, no. 3, pp. 358–370, Jun. 2009.

[4] S. R. Anton and H. A. Sodano, "A review of power harvesting using piezoelectric materials (2003–2006)," *Smart Mater. Struct.*, vol. 16, no. 3, pp. R1–R21, 2007.

[5] S. P. Beeby, M. J. Tudor, and N. M. White, "Energy harvesting vibration sources for microsystems applications," *Meas. Sci. Technol.*, vol. 17, no. 12, pp. R175–R195, 2006.

[6] D. Guyomar, A. Badel, E. Lefeuvre, and C. Richard, "Toward energy harvesting using active materials and conversion improvement by nonlinear processing," *IEEE Trans. Ultrason., Ferroelectr., Freq. Control*, vol. 52, no. 4, pp. 584–595, Apr. 2005.

[7] E. Lefeuvre, A. Badel, C. Richard, L. Petit, and D. Guyomar, "A comparison between several vibration-powered piezoelectric generators for standalone systems," *Sens. Actuators, A*, vol. 126, no. 2, pp. 405–416, 2006.

[8] Y. Liu, G. Tian, Y. Wang, J. Lin, Q. Zhang, and H. F. Hofmann, "Active piezoelectric energy harvesting: general principle and experimental demonstration," *J. Intell. Mater. Syst. Struct.*, vol. 20, no. 5, pp. 575–585, 2009.

[9] Y.-P. Liu, D. Vasic, F. Costa, W.-J. Wu, and C. K. Lee, "Velocity-controlled piezoelectric switching energy harvesting device," in *Proc. Int. Conf. Renewable Energies Power Quality*, art. no. 476 (5 pp.), 2009.

[10] W. Q. Liu, Z. H. Feng, J. He, and R. B. Liu, "Maximum mechanical energy harvesting strategy for a piezoelement," *Smart Mater. Struct.*, vol. 16, no. 6, pp. 2130–2136, 2007.

[11] J. R. Liang and W. H. Liao, "Piezoelectric energy harvesting and dissipation on structural damping," *J. Intell. Mater. Syst. Struct.*, vol. 20, no. 5, pp. 515–527, 2009.

[12] J. R. Liang and W. H. Liao, "Energy flow in piezoelectric energy harvesting systems," *Smart Mater. Struct.*, vol. 20, no. 1, art. no. 015005 (11 pp.), 2011.

[13] H. Kim, S. Priya, H. Stephanou, and K. Uchino, "Consideration of Impedance matching techniques for efficient piezoelectric energy harvesting," *IEEE Tram, Ultrason,, Ferroelectr., Freq. Control*, vol. 54, no. 9, pp. 1851–1859, Sep. 2007.

[14] J. Brufau-Penella and M. Puig-Vidal, "Piezoelectric energy harvesting improvement with complex conjugate impedance matching," *J. Intell. Mater. Syst. Struct.*, vol. 20, no. 5, pp. 597–608, 2009.

[15] N. Kong, D. S. Ha, A. Erturk, and D. J. Inman, "Resistive impedance matching circuit for piezoelectric energy harvesting," *J. Intell. Mater. Syst. Struct.*, vol. 21, no. 13, pp. 1293–1302, 2010.

[16] N. Stephen, "On energy harvesting from ambient vibration," *Sound Vib.*, vol. 293, nos. 1-2, pp. 409–425, 2006.

[17] N. Stephen, "On the maximum power transfer theorem within electromechanical systems," *J. Mech. Eng. Sci.*, vol. 220, no. 8, pp. 1261–1267, 2006.

[18] S. Koh, C. Keplinger, T. Li, S. Bauer, and Z. Suo, "Dielectric elastomer generators: How much energy can be converted?," *IEEE/ASME Trans. Mechatronics*, vol. 16, no. 1, pp. 33–41, Feb. 2011.

[19] A. Erturk and D. Inman, "On mechanical modeling of cantilevered piezoelectric vibration energy harvesters," *J. Intell. Mater. Syst. Struct.*, vol. 19, no. 11, pp. 1311–1325, 2008.

[20] M. Zhu, E. Worthington, and J. Njuguna, "Analyses of power output of piezoelectric energy-harvesting devices directly connected to a load resistor using a coupled piezoelectric-circuit finite element method," *IEEE Trans. Ultrason., Ferroelectr., Freq. Control*, vol. 56, no. 7, pp. 1309–1317, Jul. 2009.

[21] G. K. Ottman, H. F. Hofmann, A. C. Bhatt, and G. A. Lesieutre, "Adaptive piezoelectric energy harvesting circuit for wireless remote power supply," *IEEE Trans. Power Electron.*, vol. 17, no. 5, pp. 669–676, Sep. 2002.

[22] A. Wickenheiser, T. Reissman, W.-J. Wu, and E. Garcia, "Modeling the effects of electromechanical coupling on energy storage through piezoelectric energy harvesting," *IEEE/ASME Trans. Mechatronics*, vol. 15, no. 3, pp. 400–411, Jun. 2010.

[23] M. J. Guan and W. H. Liao, "On the equivalent circuit models of piezoelectric ceramics," *Ferroelectrics*, vol. 386, no. 1, pp. 77–87, 2009.

[24] A. Badel, A. Benayad, E. Lefeuvre, L. Lebrun, C. Richard, and D. Guyomar, "Single crystals and nonlinear process for outstanding vibration-powered electrical generators," *IEEE Trans. Ultrason., Ferroelectr., Freq. Control*, vol. 53, no. 4, pp. 673–684, Apr. 2006.

[25] S. Platt, S. Farritor, and H. Haider, "On low-frequency electric power generation with PZT ceramics," *IEEE/ASME Trans. Mechatronics*, vol. 10, no. 2, pp. 240–252, Apr. 2005.

[26] N. G. Elvin and A. A. Elvin, "A general equivalent circuit model for piezoelectric generators," *J. Intell. Mater. Syst. Struct.*, vol. 20, no. 1, pp. 3–9, 2009.

[27] Y. Yang and L. Tang, "Equivalent circuit modeling of piezoelectric energy harvesters," *J. Intell. Mater. Syst. Struct.*, vol. 20, no. 18, pp. 2223–2235, 2009.

[28] J. Scruggs, "An optimal stochastic control theory for distributed energy harvesting networks," *J. Sound Vib.*, vol. 320, nos. 4-5, pp. 707–725, 2009.

[29] J. Scruggs, "On the causal power generation limit for a vibratory energy harvester in broadband stochastic response," *J. Intell. Mater. Syst. Struct.*, vol. 21, no. 13, pp. 1249–1262, 2010.

[30] Y. C. Shu, I. C. Lien, and W. J. Wu, "An improved analysis of the SSHI interface in piezoelectric energy harvesting," *Smart Mater. Struct.*, vol. 16, no. 6, pp. 2253–2264, 2007.

[31] I. C. Lien, Y. C. Shu, W. J. Wu, S. M. Shiu, and H. C. Lin, "Revisit of series-SSHI with comparisons to other interfacing circuits in piezoelectric energy harvesting," *Smart Mater. Struct.*, vol. 19, no. 12, art. no. 125009 (12 pp.), 2010.

[32] G. A. Lesieutre, G. K. Ottman, and H. F. Hofmann, "Damping as a result of piezoelectric energy harvesting," *J. Sound Vib.*, vol. 269, nos. 3-5, pp. 991–1001, 2004.

[33] D. Guyomar, C. Richard, and S. Mohammadi, "Damping behavior of semi-passive vibration control using shunted piezoelectric materials," *J. Intell. Mater. Syst. Struct.*, vol. 19, no. 8, pp. 977–985, 2008.

[34] D. Guyomar, G. Sebald, S. Pruvost, M. Lallart, A. Khodayari, and C. Richard, "Energy harvesting from ambient vibrations and heat," *J. Intell. Mater. Syst. Struct.*, vol. 20, no. 5, pp. 609–624, 2009.

[35] C. B. Williams and R. B. Yates, "Analysis of a micro-electric generator for microsystems," *Sens. Actuators, A*, vol. 52, nos. 1-3, pp. 8–11, 1996.

[36] K. A. Cook-Chennault, N. Thambi, and A. M. Sastry, "Powering MEMS portable devices—A review of non-regenerative and regenerative power supply systems with special emphasis on piezoelectric energy harvesting systems," *Smart Mater. Struct.*, vol. 17, no. 4, art. no. 043001 (33 pp.), 2008.

[37] N. S. Hudak and G. G. Amatucci, "Small-scale energy harvesting through thermoelectric, vibration, and radiofrequency power conversion," *J. Appl. Phys.*, vol. 103, no. 10, art. no. 101301 (24 pp.), 2008.

[38] P. D. Mitcheson, E. M. Yeatman, G. K. Rao, A. S. Holmes, and T. C. Green, "Energy harvesting from human and machine motion for wireless electronic devices," *Proc. IEEE*, vol. 96, no. 9, pp. 1457–1486, Sep. 2008.

[39] S. Priya, "Advances in energy harvesting using low profile piezoelectric transducers," *J. Electroceram.*, vol. 19, no. 1, pp. 167–184, 2007.

[40] D. Zhu, M. J. Tudor, and S. P. Beeby, "Strategies for increasing the operating frequency range of vibration energy harvesters: A review," *Meas. Sci. Technol.*, vol. 21, no. 2, art. no. 022001 (29 pp.), 2010.

[41] A. Erturk and D. J. Inman, "Issues in mathematical modeling of piezoelectric energy harvesters," *Smart Mater. Struct.*, vol. 17, no. 6, art. no. 065016 (14 pp.), 2008.

[42] Y. C. Shu and I. C. Lien, "Analysis of power output for piezoelectric energy harvesting systems," *Smart Mater. Struct.*, vol. 15, no. 6, pp. 1499–1512, 2006.

[43] *IEEE Standard on Piezoelectricity*, ANSI/IEEE Std., 176-1987, 1988.

[44] J. R. Liang and W. H. Liao, "On the influence of transducer internal loss in piezoelectric energy harvesting with SSHI interface," *J. Intell. Mater. Syst. Struct.*, vol. 22, no. 5, pp. 503–512, 2011.

[45] M. Lallart and D. Guyomar, "An optimized self-powered switching circuit for non-linear energy harvesting with low voltage output," *Smart Mater. Struct.*, vol. 17, no. 3, art. no. 035030 (8 pp.), 2008.

[46] G. K. Ottman, H. F. Hofmann, and G. A. Lesieutre, "Optimized piezoelectric energy harvesting circuit using step-down converter in discontinuous conduction mode," *IEEE Trans. Power Electron.*, vol. 18, no. 2, pp. 696–703, Mar. 2003.

[47] M. J. Guan and W. H. Liao, "On the efficiencies of piezoelectric energy harvesting circuits towards storage device voltages," *Smart Mater. Struct.*, vol. 16, no. 2, pp. 498–505, 2007.

Junrui Liang (S'09–M'10) was born in Guangdong, China, in 1982. He received the B.E. and M.E. degrees in instrumentation engineering from Shanghai Jiao Tong University, Shanghai, China, in 2004 and 2007, respectively, and the Ph.D. degree in mechanical and automation engineering from The Chinese University of Hong Kong, Hong Kong, China, in 2010.

He is currently a Postdoctoral Fellow at The Chinese University of Hong Kong. His research interests include piezoelectric devices, energy harvesting, and Class-E power amplifiers.

Dr. Liang was a recipient of two Best Paper Awards at the IEEE International Conference on Information and Automation in 2009 and 2010. He also received the Best Student Contributions Award at the 19th International Conference on Adaptive Structures and Technologies in 2008.

Wei-Hsin Liao (M'01–SM'07) received the Ph.D. degree from The Pennsylvania State University, University Park, in 1997.

He is currently a Professor in the Department of Mechanical and Automation Engineering, The Chinese University of Hong Kong, Hong Kong, China. He is the author or coauthor of more than 120 technical papers published in international journals and conference proceedings, and holds two U.S. patents and five other patent applications. His research interests include smart structures, vibration control, energy harvesting, mechatronics, and medical devices.

Dr. Liao was the Program Chair for the International Symposium on Smart Structures and Microsystems in 2000, as well as the 2005 IEEE International Conference on Information Acquisition. He was also the Conference Chair for the 20th International Conference on Adaptive Structures and Technologies in 2009. He currently serves as an Associate Editor for the *ASME Journal of Vibration and Acoustics* as well as the *Journal of Intelligent Material Systems and Structures*, and on the Editorial Board of *Smart Materials and Structures*. He was a recipient of the T A Stewart-Dyer/F H Trevithick Prize awarded by the Institution of Mechanical Engineers in 2006, the Best Paper Award in Structures from the American Society of Mechanical Engineers in 2008, and Best Paper Awards at the IEEE International Conference on Information and Automation in 2009 and 2010. He is a Fellow of the American Society of Mechanical Engineers and the Institute of Physics.